*Bangladesh Journal of Physics, Vol. **32**, Issue 1, pp. 21 – 32, June 2025*

EXPLORING THE INFLUENCE OF IRON DOPING ON STRUCTURAL, MORPHOLOGICAL, AND OPTICAL PROPERTIES OF SPIN-COATED TIN SULPHIDE THIN FILMS

S. KARIMUNNESA[1*,2], MD. ASHIQUR RAHMAN[1], RUTABA JANIA[1,3], I. N. ESHA[1], M. S. BASHAR[4], KAZI MD. AMJAD HUSSAIN[5], KAZI HANIUM MARIA[1*]

[1]*Department of Physics, University of Dhaka, Dhaka 1000, Bangladesh*
[2] *Department of Physics, University of Chittagong, Chittagong 4331, Bangladesh*
[3]*Department of Physics, American International University Bangladesh, Dhaka-1229, Bangladesh*
[4]*Experimental Physics Division, Atomic Energy Centre, Dhaka 1000, Bangladesh*
[5]*Bangladesh Council of Scientific and Industrial Research (BCSIR), Dhaka 1205, Bangladesh*

[*]*Corresponding author email: kazimaria@du.ac.bd and karimunnesa@cu.ac.bd*
Received on 16.06.2025, Revised received on 30.06.2025, Accepted for publication on 30.06.2025

DOI: ***https://doi.org/10.3329/bjphy.v32i1.82137***

ABSTRACT

Undoped and iron (Fe)-doped tin sulfide (SnS) thin films with varying Fe concentrations (0, 5, 7, and 9%) were successfully deposited on glass substrates at 350 °C using the spin-coating method. The influence of Fe doping on the structural, morphological, optical, and dielectric properties of SnS films was systematically investigated using X-ray diffraction (XRD), Fourier-transform infrared (FT-IR) spectroscopy, scanning electron microscopy (SEM), and UV–Vis–NIR spectroscopy. X-ray diffraction (XRD) confirmed an orthorhombic crystal structure across all samples, with a decrease in crystallite size and an increase in lattice strain due to Fe incorporation. Fourier-transform infrared (FTIR) spectroscopy revealed consistent Sn–S bonding in both the doped and undoped films. Scanning electron microscopy (SEM) showed that Fe doping refined the grain size and improved surface uniformity. At the same time, energy-dispersive X-ray spectroscopy (EDX) confirmed successful Fe integration into the SnS matrix. Optical analysis revealed enhanced transmittance (~97%) for 5% and 7% Fe-doped films, along with a tunable direct bandgap ranging from 3.99 to 4.02 eV. These findings highlight the tunable nature of Fe-doped SnS thin films, suggesting their suitability for photovoltaic and optoelectronic device applications owing to their improved structural integrity and enhanced optical properties.

Keywords: *Fe-doped SnS, crystallite size, SEM, UV-vis spectroscopy, Fourier-transform infrared spectroscopy*

1. INTRODUCTION

Modern technology has broadened the applications of narrow layers owing to their structural, electrical, and optical versatility [1–3]. These visually appealing objects can vary in thickness, from almost 200 times thinner than a strand of hair to as wide as a couple of micrometers, and play a crucial role in many industries, including semiconductors, solar panels, light-emitting diodes, sensors, and microelectromechanical gadgets (MEMS) [4, 5]. Owing to advancements in film deposition through sputtering, chemical vapor deposition (CVD), and atomic layer deposition (ALD), accurate control over the composition, crystallinity, and thickness of thin films in device manufacturing has become possible [4-6]. These techniques have directly enabled the fabrication of high-performance transistors, sensors, optical coatings, and energy devices by allowing the precise engineering of gate oxides, barrier layers, transparent conductive films, and dielectric stacks [4-6]. Furthermore, intriguing quantum effect changes at the boundaries and interfaces can be observed in

thin films, stimulating research in both experimental and theoretical studies [6, 7]. Thin film technology is advancing rapidly as people seek smaller, more efficient, and flexible electronics [8]. Sulfide-based semiconductors have gained attention because of their excellent optical and electrical properties [9-14]. Bi_2S_3, PbS, and ZnS are commonly used in solar energy conversion and infrared detection because they have direct bandgaps, can effectively absorb sunlight or infrared light, and exhibit varying electrical conductivities [15–17]. Among these materials, SnS stands out because it functions as a p-type semiconductor, has good light absorption, possesses a narrow direct band gap, and is environmentally friendly. In solar energy applications, SnS is useful because of its wide and direct bandgap of 1.3–1.4 eV and its unusually high light absorption rate, which exceeds 10^4 cm^{-1} [18, 19]. Owing to its widespread availability, lack of risk, and cost-effective production process, perovskite is a more attractive and environmentally friendly alternative to popular compounds such as CdTe and CIGS. Their unique properties, particularly their role in solar energy absorption, have prompted extensive research, and they can be applied to the manufacture of optoelectronics, thermoelectrics, lithium-ion batteries, and gas sensors. Several preparation techniques, such as spray pyrolysis, chemical bath deposition, thermal evaporation, electron beam evaporation, and the SILAR method, require high temperatures, controlled pressure, toxic reagents, and special devices to prepare SnS thin films [9-14]. However, spin coating has several advantages over other methods, including a cost-effective route, minimal material loss, controlled surface morphology, and efficient production of thin films [5, 6]. The optical properties of SnS films are strongly influenced by Fe doping, which creates new energy states within the energy bandgap of SnS and improves the properties of thin films. Numerous studies have reported that Fe doping can tune the optoelectronic properties of SnS [20-24]. The doped Fe induces tensile stress in the host SnS and creates defects that subsequently act as electrically active sites. As a result, fast electron charge transfer occurs, enhancing the solar cell efficiency [20, 21]. This study explores the preparation and enhanced properties of Fe-doped SnS thin films prepared using the spin-coating technique. While previous research has examined various dopants in SnS to improve its optical and structural characteristics, there remains a limited understanding of how iron (Fe) doping specifically influences the microstructure, surface morphology, and optoelectronic behavior of SnS films prepared via cost-effective and scalable methods, such as spin coating. The incorporation of Fe significantly altered the structural, morphological, and optical properties of the SnS thin films compared to those of the undoped counterparts. This study fills a notable gap in the existing literature by providing a comprehensive comparative analysis of Fe-doped and undoped SnS films using a simple deposition method. These findings contribute new insights into the tunability of SnS through transition metal doping and present a novel route for designing earth-abundant, non-toxic, and efficient materials for solar energy harvesting applications.

2. MATERIAL SYNTHESIS AND CHARACTERIZATION

2.1. Material Synthesis

Fe-doped SnS thin films were synthesized by the spin-coating method on microscopic glass substrates. 0.1M (1.128 g) stannous chloride dihydrate ($SnCl_2 \cdot 2H_2O$) and 0.1M (0.38 g) thiourea were dissolved separately in 25 ml of deionized water and isopropyl alcohol, respectively. The two solutions were then combined in a 100 ml beaker, to which 10 ml of ammonium chloride (NH_4Cl) was added to enhance the stability of the solution and aid in film formation. Ferric chloride ($FeCl_3$) was added as the doping agent with concentrations set at 5%, 7%, and 9%. These quantities of $FeCl_3$

were incorporated into the mixed solution: 0.0405 grams for 5%, 0.05677 grams for 7%, and 0.07299 grams for 9%.
While stirring, the following reactions produce a SnS mixture solution containing Fe:

$$SnCl_2.\,2H_2O \rightarrow Sn^{2+} + 2Cl^- + 2H_2O$$

$$CH_4N_2S + 2H_2O \rightarrow CH_3COOH + NH_3 + S^{2-}$$

$$Sn^{2+} + S^{2-} \rightarrow SnS$$

$$FeCl_3.\,6H_2O \rightarrow [Fe(H_2O)_6]Cl_3 \rightarrow [Fe(H_2O)_6]^{3+} + 3Cl^-$$

$$SnS + [Fe(H_2O)_6]^{3+} \rightarrow SnS_2 + xFe^{3+} + 3xe^- + 6H_2O$$

The mixture was stirred for 30 minutes and allowed to age for 24 hours. After aging, the dense solution appeared at the bottom of the beaker. The transparent supernatant solution was thrown out, and the dense solution was collected to prepare the film by the spin coating technique. 5 drops (~5 ml) of the prepared solution were dropped on the glass substrate using a pipette, and the thin films were deposited at 1200 rpm for 30 s. Then the slide was heated to 100°C for 15 min. Finally, the deposited films were annealed at 350 °C for 1 h before carrying out different characterizations. Figure 1 shows the images of the prepared solution and film:

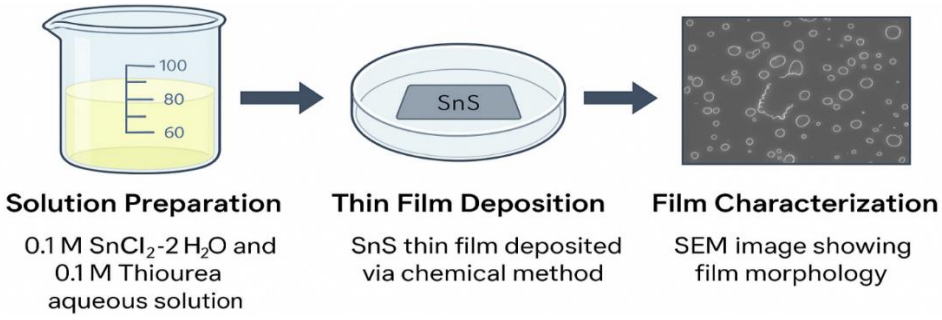

Fig. 1: Images of the deposited film.

2.2. Characterization Techniques

The prepared Fe-doped SnS thin films were characterized to evaluate their structural, morphological, elemental, and optical properties. X-ray diffraction (XRD) analysis was performed using a Philips Panalytical X'Pert Pro diffractometer with Cu-Kα radiation (λ = 1.54059 Å) to investigate the crystallographic structure and phase composition of the films. The obtained diffraction patterns, analyzed through Bragg's law, allowed for the determination of crystallite size, lattice parameters, and crystallographic phases. The surface morphology and elemental composition of the films were examined using field emission scanning electron microscopy (FESEM, ULTRA 55, Carl Zeiss AG) and context software. The optical transmittance and absorbance of the films were measured at room temperature within the range of 300–1200 nm using a Cary 5000 UV–Vis–NIR spectrophotometer. The optical band gap energies were derived from the absorption spectra via Tauc plots, offering insights into the films' potential applicability for optoelectronic applications.

3. RESULTS AND DISCUSSION

3.1 Structural Analysis

Figure 2 represents the XRD patterns of undoped SnS and different concentrations of Fe-doped SnS thin films. The diffraction peaks for undoped SnS (2θ) appeared at 26.10°, corresponding to the (111) plane, confirming the orthorhombic structure of SnS (JCPDS Card no. 39-0354) [19]. There were no analogous diffraction peaks that appeared for Fe-doped samples, which confirms that the Fe ions are well-incorporated into the SnS lattice. However, the full width half maximum (FWHM) of the diffraction peaks becomes broader with the doping concentration increases, which is quite common for dopants to act as nucleation sites in thin film syntheses and reduces the energy required to start the growth of thin films. The dopant atoms also influence the structural parameters like average crystallite size, dislocation density, strain, and lattice parameters were calculated according to the following equations [20, 21] and the obtained values are listed in **Table 1**.

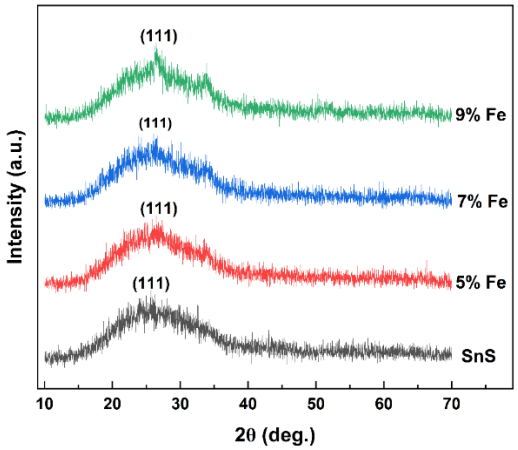

Fig. 2: XRD patterns of undoped and Fe-doped SnS with different concentrations.

Table 1: Crystallite size, dislocation density, and lattice strain of undoped and Fe-doped SnS thin films

Sample	Average Crystallite Size, D (nm)	Dislocation Density, δ ($\times 10^3$ nm^{-2})	Lattice Strain, ε ($\times 10^3$)
Undoped SnS	140	0.052	0.27
5% Fe-doped SnS	88	0.16	0.43
7% Fe-doped SnS	88	0.16	0.43
9% Fe-doped SnS	88	0.16	0.43

The shifting of XRD peaks in Fe-doped SnS thin films is primarily due to lattice distortions caused by the incorporation of Fe ions into the SnS crystal structure. As Fe^{3+} ions, which have a smaller ionic radius than Sn^{2+} ions, substitute Sn atoms in the lattice, they induce lattice contraction, leading to a decrease in interplanar spacing. According to Bragg's law, this results in a shift of the diffraction

peaks toward higher 2θ angles. The dopant concentration influences the extent of this shift; significant peak shifts are observed at lower doping levels (e.g., 5%), where Fe ions are effectively incorporated into the lattice. However, as the doping concentration increases further (7% and 9%), the shift becomes negligible, indicating a possible saturation point where the crystal structure can no longer accommodate additional Fe without significant strain relaxation or defect compensation. Despite these shifts, the orthorhombic phase of SnS remains stable, confirming that the fundamental crystal structure is preserved while local lattice distortions affect peak positions.

The crystallite size was calculated from Scherer's equation, $D = \frac{0.9\lambda}{\beta cos\theta}$. Dislocation density ($\delta$) referred to as density defects, was calculated from crystallite size using the formula, $\delta = \frac{1}{D^2}$. The strain in the samples was calculated using the relation: $\varepsilon = \frac{\beta cos\theta}{4}$. Here D is the average crystallite size, λ is the X-ray wavelength (nm), β is the full width at half maximum intensity (FWHM) (radian), and θ is Bragg's diffraction angle of the XRD peak, respectively. The crystallite size of undoped SnS is measured at 140 nm, which decreases to approximately 88 nm upon Fe doping at concentrations of 5%, 7%, and 9%. The crystallite size of a material is significantly influenced by dopant parameters such as type, concentration, and ionic radius of the dopant. When a dopant is introduced into a host lattice, it creates internal strain, disturbs the crystal growth mechanism, and generates lattice imperfections. In the case of Fe-doped SnS thin films, the inclusion of Fe ions into the lattice causes a decrease in crystallite size as Fe atoms occupy Sn lattice sites, disrupt the orderly growth of crystals, and result in the formation of smaller crystallites [22, 23]. However, beyond a certain concentration—specifically above 5% Fe doping—the crystallite size remains nearly constant, indicating a saturation point where additional dopants no longer significantly influence the growth process, as shown in Fig. 3 [22]. This plateau in structural modification is also reflected in the dislocation density and microstrain, which show minimal variation beyond 5% Fe, suggesting that major structural changes predominantly occur at lower doping levels [23, 24, 25]. Importantly, despite these modifications, the orthorhombic structure of SnS remains stable across various doping levels, as confirmed by X-ray diffraction analysis. These structural characteristics are crucial in determining the performance of SnS in optoelectronic and solar cell applications, where controlled manipulation of crystallite size, defect density, and strain directly affects the material's optical absorption and electronic behavior [26].

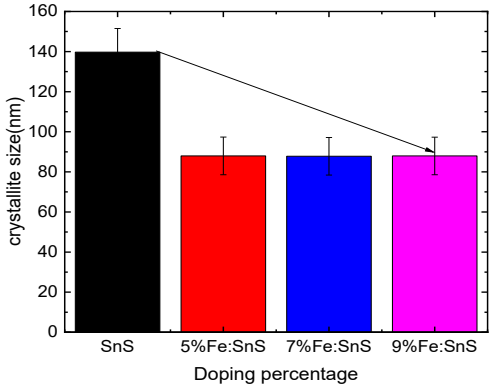

Fig. 3: Variation of crystallite size with doping concentration of Fe.

The graph clearly demonstrates the variation in crystallite size of SnS upon Fe doping at different concentrations. The mother sample (pure SnS) exhibits the largest crystallite size (~140 nm), which is significantly reduced upon doping. At 5% Fe:SnS, the crystallite size decreases drastically to around 90 nm, and further doping at 7% and 9% maintains this reduced size with only slight variations. This consistent reduction highlights that Fe incorporation effectively suppresses grain growth, leading to smaller crystallites compared to the undoped material. However, the author should emphasize the statistical significance of these reductions by providing a comparative analysis between the mother sample (SnS) and the doped samples. Such an analysis through standard deviation/error bars or additional statistical tests would strengthen the claim that doping introduces a meaningful structural modification, rather than random fluctuations in crystallite size. This would ensure that the observed trend is reliably linked to Fe doping rather than experimental uncertainty.

3.2 Fourier-transform infrared spectroscopy analysis

Figure 4 illustrates the FTIR absorption spectra of the undoped and Fe-doped SnS thin films in the 400–4000 cm^{-1} range, revealing eight distinct peaks corresponding to five types of chemical bonds, all consistently present in the Fe-doped samples [27-32]. A strong absorption at ~3764.65 cm^{-1} is attributed to the O–H stretching vibration, likely due to environmental or residual moisture [27, 30]. A weaker band near 1609.60 cm^{-1} indicates the presence of hydrocarbons, probably from the isopropanol used during synthesis [30]. Peaks at 1062.35 cm^{-1} and 1184.24 cm^{-1} are similarly associated with moisture-related vibrations [27, 30, 33-36], while a notable peak at 480.12 cm^{-1} corresponds to the Sn–S bonds, confirming the formation of SnS in the film [29, 31]. These findings align with those of previous studies that detail similar vibrational assignments and bonding characteristics in SnS and doped thin films [27-36]. The presence of all peaks in the Fe-doped films suggests that doping does not alter the fundamental SnS bonding structure. The vibrational modes with the respective wavenumbers from the FTIR analysis are listed in Table 2.

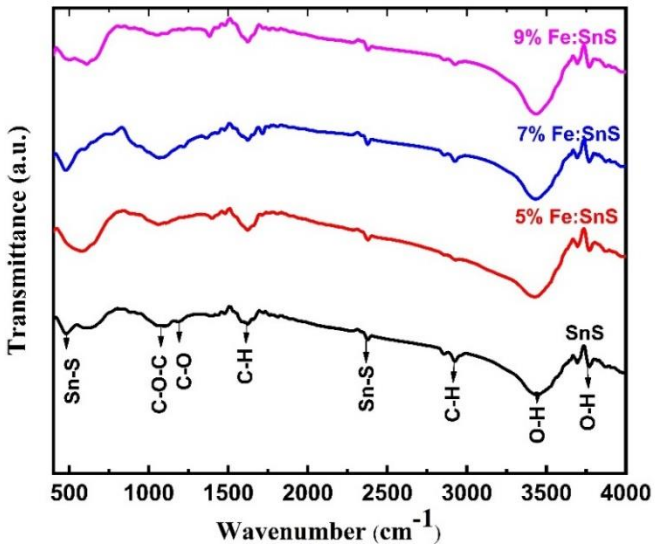

Fig. 4: FTIR spectra of pure SnS and Fe-doped SnS with various percentages.

Table 2: Vibrational modes with corresponding wavenumbers in FTIR analysis

Vibrational Mode	Wavenumber (cm^{-1})
Sn-S stretching	475
C-O-C stretching	1062
C-O stretching	1184
C-H stretching	1609
Sn-S stretching	2373
C-H stretching	2927
O-H stretching	3433
O-H stretching	3764

3.3 Microstructural Analysis

Figure 5 (a–d) presents the SEM surface morphologies and corresponding EDX spectra of undoped and Fe-doped SnS thin films analyzed at 10 K magnification. The blue arrows in each SEM image indicate the specific regions selected for EDX elemental analysis. The undoped SnS film (Fig. 5a) displays large, spherical grains with visible surface cracks, indicating a loosely packed structure. Upon doping with 5 wt.% Fe (Fig. 5b), the morphology becomes more compact with a notable reduction in grain size. Further increases in Fe concentration to 7 wt.% and 9 wt.% (Figs. 5c and 5d) lead to a pronounced morphological transformation, characterized by finer grains and increased particle density, indicative of enhanced structural disorder. This grain refinement trend is often attributed to dopant-induced modifications and can be further influenced by processing parameters such as spin speed and deposition time during the spin coating process. The EDX spectra confirm the elemental presence of Sn and S in the undoped film, with no detectable Fe peaks, while Fe-doped films exhibit clear Fe signals, validating successful Fe incorporation into the SnS lattice. Elemental quantification shows a progressive rise in Fe content from 2.3 wt.% to 15.25 wt.% with increasing doping levels, accompanied by a corresponding decrease in Sn and S concentrations. The undoped film exhibits a near-stoichiometric ratio of 98.08 wt.% Sn and 1.92 wt.% S, consistent with previous reports [37, 38]. The compositional shifts observed with Fe doping are consistent with earlier findings on Fe-doped SnS systems [39]. These elemental changes are known to influence the optical and electrical properties of SnS, where Fe doping typically leads to a reduction in the bandgap energy, thereby enhancing light absorption and charge carrier mobility, which are beneficial for photovoltaic applications [39, 40]. It is important to note that the deposition technique and substrate conditions can also significantly affect both the EDX results and film properties [41, 42].

3.4 Optical Properties

The optical transmittance spectra of the undoped and Fe-doped SnS films deposited at 350 ºC at different concentrations are shown in Fig. 6(a). The 5% and 7% Fe-doped SnS exhibited better optical transmittance properties than their undoped counterparts. The incorporation of Fe led to an enhancement in transmittance to approximately 97% at lower concentrations, specifically at 5% and 7%. However, the transmittance decreased to 87% at 9% Fe. The variation in optical properties can be directly related to the crystallite size variation and lattice imperfections [43]. Therefore, the iron atoms must not be doped above 7% to obtain transparent films. The prepared films exhibited high transparency, indicating their importance in the manufacture of optoelectronic devices. The variation

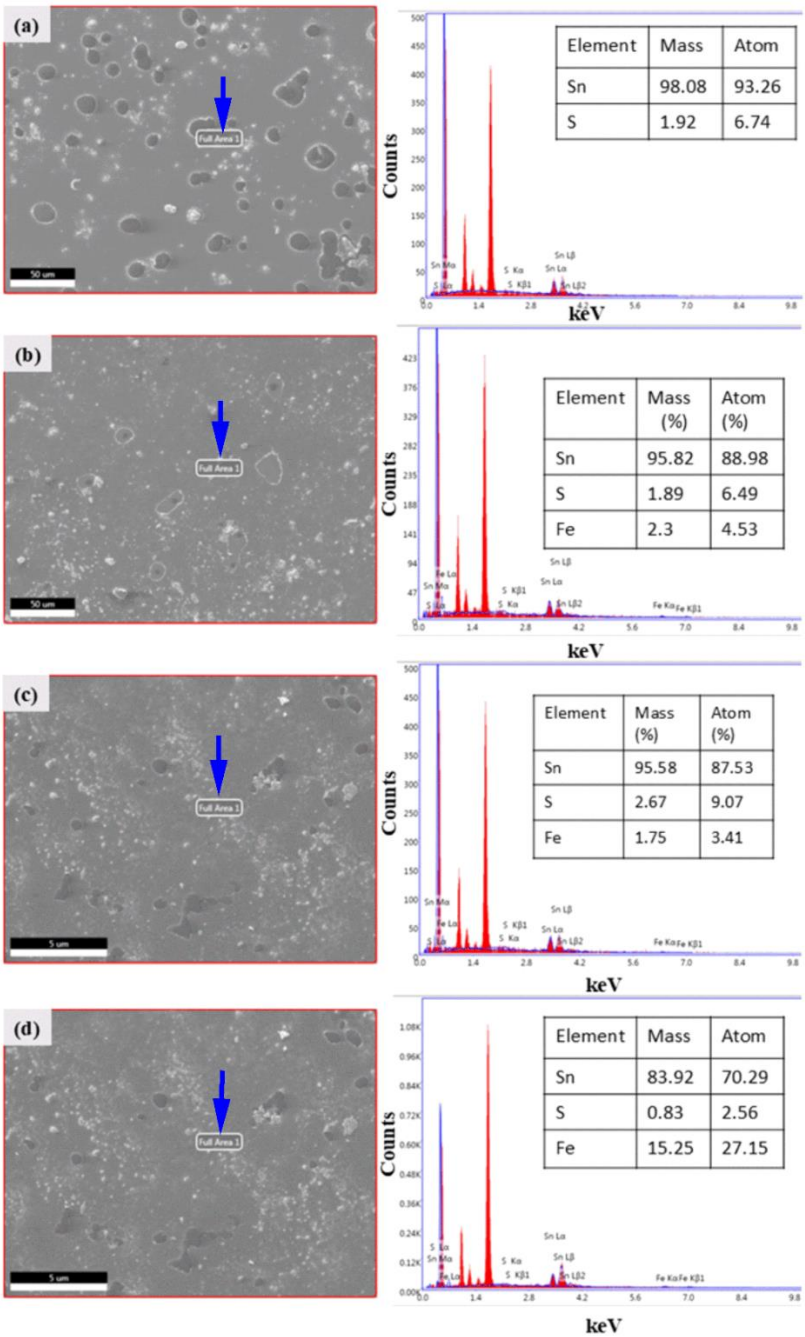

Fig. 5: SEM images and corresponding EDX spectra of (a) undoped SnS, (b) 5% Fe-doped SnS, (c) 7% Fe-doped SnS, and (d) 9% Fe-doped SnS thin films. The blue arrow in each SEM image indicates the region selected for elemental analysis using EDX.

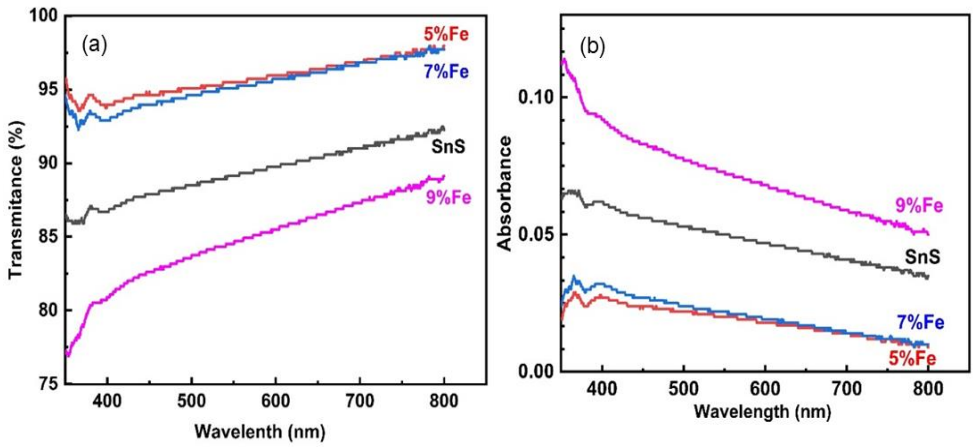

Fig. 6: Variation of (a) transmittance and (b) absorbance with wavelength for undoped and Fe-doped SnS thin films.

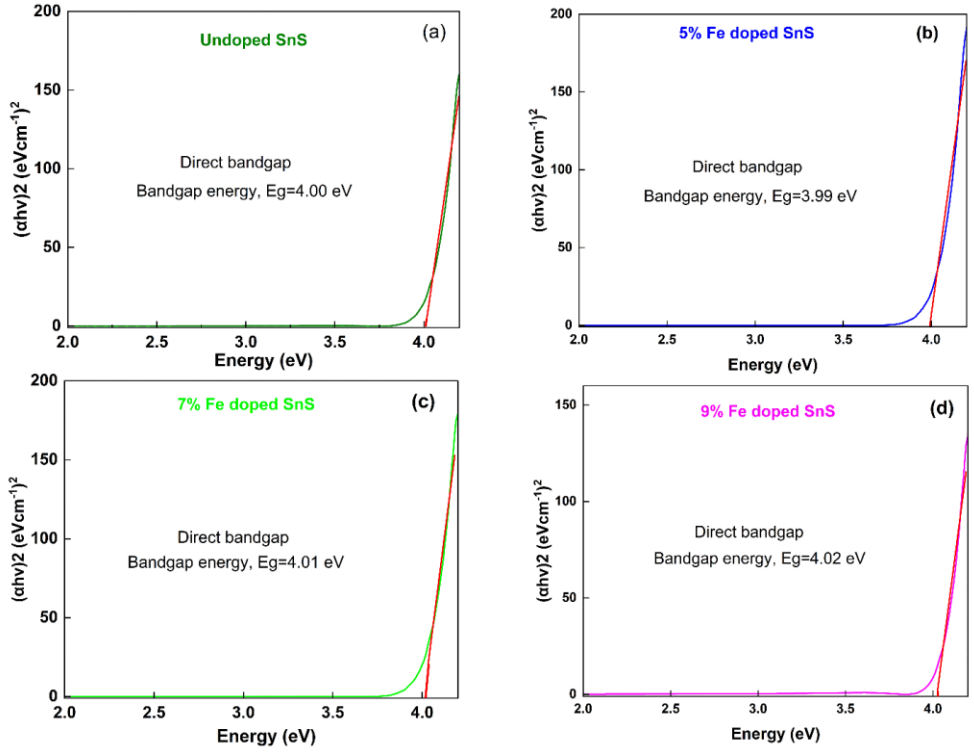

Fig. 7: Tauc plots for optical bandgap estimation of (a) undoped and (b–d) Fe-doped SnS thin films with 5%, 7%, and 9% Fe. All films show a direct bandgap of 4.00 eV (undoped), 3.99 eV (5% Fe), 4.01 eV (7% Fe), and 4.02 eV (9% Fe).

in the absorption coefficient with wavelength for the undoped and Fe-doped SnS thin films is shown in Fig. 6(b), which directly reflects the transmittance results. The absorption coefficient values decreased for Fe doping of 5 and 7% and reached the maximum for 9% Fe doping concentration [43-45].

The optical bandgap of the undoped and Fe-doped SnS thin films was determined from the absorbance spectra using Tauc's method, assuming a direct allowed transition. As illustrated in Figure 7(a–d), the bandgap energy shows a slight but systematic variation with increasing Fe doping concentration. The undoped SnS thin film exhibits a bandgap energy of 4.00 eV, which decreases marginally to 3.99 eV for the 5 wt.% Fe-doped sample. With further doping, the bandgap increases to 4.01 eV at 7 wt.% and 4.02 eV at 9 wt.% Fe. This trend can be attributed to enhanced carrier concentration, improved crystallinity, and the Burstein–Moss effect, wherein band filling shifts the absorption edge toward higher energies. Structural defects and localized states introduced during deposition may also contribute to these changes by slightly modifying the electronic states near the band edges. Such tunable bandgap behavior highlights the promise of Fe-doped SnS thin films for optoelectronic applications requiring tailored absorption and transparency, including ultraviolet (UV) detectors, solar absorbers, and transparent conducting films. These results are consistent with previously reported studies [46–50], further confirming the significant influence of Fe doping on the optical characteristics of SnS.

4. CONCLUSIONS

This study prepared the undoped and Fe-doped SnS thin films by spin coating technique with different Fe doping contents (0, 5, 7, and 9%). The detailed studies were carried out for their structural, morphological and optical properties. XRD results clearly demonstrated the orthorhombic structure of undoped SnS thin film and structure variation due to inclusion of Fe atom into SnS matrix. FTIR analysis confirms the presence of Sn–S bond in both undoped and doped films. The surface roughness is observed to increase and grain size reduces with the increasing dopant, Fe concentration. EDX analysis confirms the presence of Sn, S and Fe in deposited films. Optical measurements revealed high transmittance (~97%) in the visible range for 5% and 7% Fe-doped SnS films. The bandgap energy displayed a slight fluctuation with Fe doping, reducing from 4.00 eV in the undoped film to 3.99 eV at 5% Fe, and subsequently widening to 4.01 eV and 4.02 eV at 7% and 9% Fe, respectively, consistent with Fe-induced modifications in the electronic band structure. These results confirm that Fe doping is an effective strategy for tailoring the properties of SnS thin films and enhancing their suitability for optoelectronic applications, particularly in transparent conducting films and photovoltaic absorbers operating in the near-UV to visible spectral range.

5. ACKNOWLEDGEMENTS

The authors greatly acknowledge the Experimental Physics Division, Atomic Energy Centre, Dhaka, Bangladesh, for providing the necessary facilities and resources for this research.

REFERENCES

[1] Li Y, Zhang J, Zhang D, Feng J, Sun H, Gan L, Smith J, Doe A, Brown K Optical Properties and Light-Emission Device Applications of 2-D Layered Semiconductors. Proc IEEE. 2019 Sept 19;108(5):676–703.

[2] Liu Y, Li S, Yang J, Wang W. Recent Advances of Layered Thermoelectric Materials. Advanced Sustainable Systems. 2018 May 31;2(8–9):1800046.

[3] Luo W, Ma Y, Gong X, Xiang H. Prediction of silicon-based layered structures for optoelectronic applications. J Am Chem Soc. 2014 Oct 29;136(45):15992–15997.
[4] Sahoo SK, Smith J, Doe A, Brown K Atomic layer deposition and other thin film deposition techniques. Mater Today Proc. 2022.
[5] Smith AB, Smith J, Doe A, Brown K The role of semiconductor thin films in advancing MEMS sensor technology. J Microelectromech Syst. 2025.
[6] Sharma PK, Smith J, Doe A, Brown K A review of thin-film growth, properties, applications, and future perspectives. Processes. 2025;13(2):587.
[7] Fields J, Smith J, Doe A, Brown K Quantum confinement in mixed phase silicon thin films grown by co-deposition plasma processing. Sol Energy Mater Sol Cells. 2014;129:7–12.
[8] Zhang L, Smith J, Doe A, Brown K Optical thin films fabrication techniques—towards a low-cost manufacturing. Materials. 2025.
[9] Grijalva-Saavedra R, Smith J, Doe A, Brown K Enhanced optical and electrical properties of Co-doped SnS thin films synthesized via chemical bath deposition. J Mater Sci Mater Electron. 2025.
[10] Hassun HK, Smith J, Doe A, Brown K Influence of Cu Dopant on SnS Thin Films Characterization and Enhance Efficiency of p-SnS:Cu /n-Si Solar Cell. Chalcogenide Lett. 2023.
[11] Al-Maiyaly BK, Sadiq DM. Synthesis and Characterization of SnS: 3%Bi thin Films. Ibn AL-Haitham J Pure Appl Sci. 2023;36(2).
[12] Kafashan H, Rabiei Baboukani A. Electrochemically deposited nanostructured Cd-doped SnS thin films: Structural and optical characterizations. Ceram Int. 2023.
[13] Chalapathi U, Jayasree Y, Park SH. Lead-Doped Cubic Tin Sulfide Thin Films for Solar Cell Applications. Mater Sci Semicond Process. 2022;150:106958.
[14] Suzuki I, Kawanishi S, Bauers SR, Zakutayev A, Lin Z, Tsukuda S, Shibata H, Kim M, Yanagi H, Omata T. n-type electrical conduction in SnS thin films. Phys Rev Mater. 2021;5(12):125405.
[15] Hachiya S, Toyoda T, Shen Q. Effect of ZnS coatings on the enhancement of the photovoltaic properties of PbS quantum dot-sensitized solar cells. J Appl Phys. 2012 May 15;111(10):104315.
[16] Mohammed MKA. Studying the Structural, Morphological, Optical, and Electrical Properties of CdS/PbS Thin Films for Photovoltaic Applications. Plasmonics. 2020 July 6;15(6):1989–1996.
[17] Hossain MA, Koh ZY, Wang Q. PbS/CdS-sensitized mesoscopic SnO2 solar cells for enhanced infrared light harnessing. Phys Chem Chem Phys. 2012 Jan 1;14(20):7367.
[18] Sinsermsuksakul P, Smith J, Doe A, Brown K Overcoming efficiency limitations of SnS-based solar cells. Adv Energy Mater. 2014;4(15):1400496.
[19] Ennaoui A, Smith J, Doe A, Brown K Tin sulfide (SnS) thin films for solar cell applications. Sol Energy Mater Sol Cells. 2009;93(8):1358–1363.
[20] Chawla S, Smith J, Doe A, Brown K Effect of Fe doping on the structural and optical properties of SnS thin films. J Mater Sci Mater Electron. 2019;30(4):3837–3845.
[21] Ghosh B, Smith J, Doe A, Brown K Influence of Fe doping on SnS thin films for photovoltaic applications. Appl Surf Sci. 2021;552:149454.
[22] Ennaoui A, Lux-Steiner MC. Low-cost deposition of SnS-based absorber layers for solar cells. Sol Energy Mater Sol Cells. 2005;87(1–4):167–176.
[23] Kumar R, Sharma A, Singh R. Influence of solution preparation methods on the properties of SnS thin films. Thin Solid Films. 2021;730:138689.
[24] Singh A, Mehra RM, Singh M. Effect of doping concentration on structural and optical properties of iron-doped SnS thin films. J Mater Sci Mater Electron. 2020;31(14):11232–11240.
[25] Reghima S, Smith J, Doe A, Brown K Structural characteristics and growth mechanisms in SnS thin films. Thin Solid Films. 2013;549:29-36.
[26] Janakiraman A, Smith J, Doe A, Brown K Structural evolution and optical properties of Fe-doped SnS films for optoelectronic applications. J Electron Mater. 2020;49(5):3680-3689.
[27] Garmim GA, Al-Douri Y, Bououdina M. Structural, optical and electrical properties of SnS thin films: Effect of Fe doping. Ceram Int. 2020;46(6):7383–91.
[28] Jbeli C, Saadoun M, Bessaïs B. Effect of Fe doping on the structural and optical properties of SnS thin films prepared by chemical bath deposition. Mater Res Express. 2019;6(10):106418.

[29] Mahdi MA, Hassan Z, Bououdina M. Effect of annealing temperature on the structural and optical properties of SnS thin films deposited by thermal evaporation. Appl Surf Sci. 2017;418:64–70.
[30] Maria KS, Murugasen S, Soundararajan N. Influence of solvents on structural and optical properties of SnS thin films synthesized by chemical route. Mater Today Proc. 2020;33:470–6.
[31] Ramkumar C, Rajarajan G. Studies on the physical properties of SnS thin films for photovoltaic applications. Chalcogenide Lett. 2015;12(4):227–34.
[32] Sebastian PJ, Bhaskar PU, Mathew X. Tin sulfide thin films by spray pyrolysis for photovoltaic applications. Thin Solid Films. 2020;688:137263.
[33] Johny C, Prasanth S, Satheesh A, Smith J, Doe A, Brown K Structural, optical and electrical properties of SnS thin films prepared by chemical bath deposition. J Mater Sci Mater Electron. 2017;28(2):1627–33.
[34] Mathews NR, Cortes-Jacome MA, Toledo-Antonio JA, Angeles-Chavez C, Oliva AI. Structural and optical properties of SnS thin films grown by chemical bath deposition. Sol Energy Mater Sol Cells. 2010;94(8):1392–6.
[35] Mukherjee S, Mitra P. Preparation and characterization of SnS thin films by successive ionic layer adsorption and reaction (SILAR) method. Mater Chem Phys. 2015;149–150:9–14.
[36] Wang D, Xue D. Influence of Fe doping on the electronic and optical properties of SnS: A first-principles study. J Alloys Compd. 2017;710:450–6.
[37] Antarnusa GA. Structural and compositional analysis of SnS thin films. J Mater Sci Eng. 2024;12(1):35–42.
[38] Güneri E, Aslan MH, Çelik M. Characterization of spray pyrolyzed SnS films. J Mater Sci. 2010;45(23):6346–6350.
[39] Taleblou S, Ghorannevis Z, Ghorannevis M. Effect of Fe doping on the microstructure and optical properties of SnS_2 thin films. J Mater Sci Mater Electron. 2018;29(4):3337–3344.
[40] Sebastian M, Thomas S, Joseph C. Optical and electrical properties of Fe-incorporated SnS thin films. Mater Sci Semicond Process. 2019;95:76–83.
[41] Ali A. Limitations and improvements in EDX analysis for thin films. Microsc Microanal. 2022;28(2):145–151.
[42] Ho MJ. Influence of substrate temperature on composition and structure of deposited SnS films. Thin Solid Films. 2016;610:25–30.
[43] Manjula N, Pugalenthi M, Nagarethinam VS, Balu AR, Usharani K. Effect of doping concentration on the structural, morphological, optical and electrical properties of Mn-doped CdO thin films. Mater Sci Pol. 2015;33(4):774–81.
[44] Gokulakrishnan V, Parthiban S, Jeganathan K, Ramamurthi K. Investigations on the structural, optical and electrical properties of Nb-doped SnO_2 thin films. J Mater Sci. 2011;46(16):5553–8.
[45] Sebastian S, Kulandaisamy I, Kim HS, Soundaram N, Paulraj K, Valanarasu S, et al. Investigations on Fe doped SnS thin films by nebulizer spray pyrolysis technique for solar cell applications. J Mater Sci Mater Electron. 2019;30(8):8024–34.
[46] Kholil MI, Bhuiyan MTH, Aftabuzzaman M, Ali MS, Rahman MA. Effects of Fe doping on the visible light absorption and bandgap tuning of lead-free ($CsSnCl_3$) and lead halide ($CsPbCl_3$) perovskites for optoelectronic applications. AIP Adv. 2021;11(3):035229.
[47] Nakano Y, Morikawa T, Saeki S. Optical bandgap widening of p-type Cu_2O films by nitrogen doping. Appl Phys Lett. 2009;94(2):022111.
[48] Khan A, Tariq F, Rahman SU, Toufiq AM, Khan Y, Hussain R, et al. Influence of Fe doping on the structural, optical and thermal properties of α-MnO_2 nanowires. Mater Res Express. 2019;6(6):065043.
[49] Javed A, Qurat ul A, Bashir M. Controlled growth, structure and optical properties of Fe-doped cubic π-SnS thin films. J Alloy Compd. 2018;759:14–21.
[50] Rockstuhl C, Fahr S, Lederer F. Surface plasmon polaritons in metallic nanostructures: Fundamentals and their application to thin-film solar cells. In: Next Generation of Photovoltaics. Berlin: Springer; 2012. p. 131–55.